Crystal Dynamics of Lead. I. Dispersion Curves at 100°K

B. N. BROCKHOUSE,* T. ARASE,† G. CAGLIOTI,‡ K. R. RAO,§ AND A. D. B. WOODS
Neutron Physics Branch, Atomic Energy of Canada Limited, Chalk River, Ontario, Canada

(Received June 4, 1962)

Frequency/wave vector $\nu(\mathbf{q})$ dispersion curves for lead at 100°K have been measured by neutron spectrometry along the lines $[\zeta 00]$, $[\zeta\zeta\zeta]$, and $[\zeta 10]$ in the reduced zone. The experiments were performed with the triple-axis crystal spectrometer, making extensive use of the "constant **Q**" method. The results show many interesting features. The dispersion relations have local *minima* at the point (1,0,0), leading to extra critical points in the frequency distribution. The dispersion curves are analyzed into Fourier components (within the estimated errors), according to the equation $M\omega^2=\Sigma_{n=1}^{N}\Phi_n[1-\cos(\pi nq/q_M)]$ with $N\leq 12$. The existence of high Fourier components is definitely established. These high Fourier components imply the existence of very long range forces between the atoms in lead. In some cases the forces are of alternating sign. The dispersion curves show small anomalies which are believed to arise from the effect predicted by Kohn. The positions in reciprocal space at which these anomalies occur agree well with the quasi-free model for the electrons in lead, proposed by Gold. In the [111] direction (extended zone scheme) the Fermi radius is less than 1% greater than the free electron value of $1.24(2\pi/a)$; in the [110] direction the Fermi radius is $(1.19\pm 0.01)(2\pi/a)$. The Kohn effect is discussed in terms of theoretical work of Bardeen and Toya and the reasons for its observability in Pb are elucidated.

I. INTRODUCTION

THE frequency/wave vector dispersion relations of the lattice vibrations in lead have been studied extensively at this laboratory[1–4] using neutron spectrometry.[5] The work forms part of a program on the crystal dynamics of metals in which two elements which are strictly metallic but of very different properties have been examined, sodium[6] and lead.

In this paper we summarize the measurements on lead described earlier,[1–3] and present new experimental results. The results show that the frequency/wave vector dispersion relation for the lattice vibrations depends sensitively on the detailed electronic structure of the metal. In particular an effect predicted by Kohn[7] was found[3] for the first time: Anomalies in the dispersion curves were observed which can be related to the Fermi surface. In the paper some implications of the results for the Fermi surface of lead are discussed.

In the course of the work, it was discovered[8] that the neutron groups at the higher temperatures are markedly energy broadened. (The effect was independently discovered in aluminium by Larsson, Dahlborg, and Holmryd).[9] This broadening was interpreted[2,8] as arising from the lifetimes of the phonons via the uncertainty principle. On this interpretation the lifetimes turn out to be remarkably short, of the order of a vibrational period at the higher temperatures. This work will be discussed in a succeeding paper.[8]

The dispersion curves depend rather directly on the harmonic forces existing between ions in the crystal, while the phonon lifetimes depend on the anharmonic forces. For a sufficiently simple crystal it is possible to deduce the harmonic forces from the dispersion curves by use of the Born-von Kármán theory[10] of crystal dynamics.

In the Born-von Kármán theory[10] the atomic motions in a crystal are described by lattice waves which are considered to be uncoupled harmonic oscillators (normal modes). The frequencies of the oscillators are related to their wave vectors **q** (of magnitude 2π/wavelength) by the dispersion relation

$$\nu=\nu_j(\mathbf{q}), \tag{1}$$

where the j signifies the branch and takes on three values in the case of lead, a face-centered cubic crystal. The dispersion relation can be determined directly by means of neutron spectrometry, by study of the process in which neutrons interact with the crystal by creation or annihilation of a single phonon (quantum of a normal mode). The frequency and wave vector of the particular normal mode are determined from conser-

---

* Present address: Department of Physics, McMaster University, Hamilton, Ontario, Canada.

† Visitor (1958) from the Hudson Laboratories of Columbia University, supported by the U.S.O.N.R. Part of this work was included in a Ph.D. thesis (1959) for New York University.

‡ Visiting scientist (1959) from Comitato Nazionale Energia Nucleare, Roma, Italy. Now at C.C.R. Euratom, Italy.

§ Visiting scientist (1961) from Atomic Energy Establishment, Trombay, Bombay, India; now returned.

[1] T. Arase, B. N. Brockhouse, G. Caglioti, and A. D. B. Woods, Bull. Am. Phys. Soc. **5**, 39 (1960); T. Arase, thesis, New York University, 1959.

[2] B. N. Brockhouse, T. Arase, G. Caglioti, M. Sakamoto, R. N. Sinclair, and A. D. B. Woods, *Inelastic Scattering of Neutrons in Solids and Liquids* (International Atomic Energy Agency, Vienna, 1961), p. 531.

[3] B. N. Brockhouse, K. R. Rao, and A. D. B. Woods, Phys. Rev. Letters **7**, 93 (1961).

[4] A. D. B. Woods and B. N. Brockhouse, Bull. Am. Phys. Soc. **7**, 63 (1962).

[5] B. N. Brockhouse, reference 2, p. 113.

[6] A. D. B. Woods, B. N. Brockhouse, R. H. March, A. T. Stewart, and R. Bowers, following paper [Phys. Rev. **128**, 1112 (1962)].

[7] W. Kohn, Phys. Rev. Letters **2**, 393 (1959).

[8] B. N. Brockhouse, G. Caglioti, M. Sakamoto, R. N. Sinclair, and A. D. B. Woods, Bull. Am. Phys. Soc. **5**, 39 (1960); and to be published.

[9] K.-E. Larsson, U. Dahlborg, and S. Holmryd, Arkiv Fysik **17**, 369 (1960). Also, reference 2, p. 587.

[10] See M. Born and K. Huang, *Dynamical Theory of Crystal Lattices* (Oxford University Press, New York, 1954).

vation of energy and quasi-momentum between the neutron and the phonon. The incoming and outgoing neutron wave vectors ($\mathbf{k}_0,\mathbf{k}'$) and energies (E_0,E') are related to the phonon wave vector and energy by means of the equations,[11]

$$\mathbf{Q}\equiv\mathbf{k}_0-\mathbf{k}'=2\pi\boldsymbol{\tau}-\mathbf{q}, \tag{2a}$$

$$E_0-E'=\pm h\nu=\pm\hbar\omega, \tag{2b}$$

where $\boldsymbol{\tau}=a^{-1}(h,k,l)$ is a vector of the reciprocal lattice, a is the cubic lattice constant (4.924 Å for Pb at 100°K), and (h,k,l) are a set of Miller indices. Thus, scattered neutrons occur as groups in the energy distribution which, neglecting resolution, are ideally sharp. The centers of the neutron groups, when used with Eq. (2), give values for the frequency ν and wave vector $\mathbf{q}$ of the phonons with which the neutrons interacted.

The integrated intensities of these neutron groups are proportional to the expression[11]

$$A=\frac{k'}{k_0}\begin{Bmatrix} N_j \\ N_j+1 \end{Bmatrix}\exp(-Q^2u^2)\frac{(\mathbf{Q}\cdot\boldsymbol{\xi}_j)^2}{\nu_j}, \tag{3}$$

where $\boldsymbol{\xi}_j$ is the polarization vector of the normal mode, $\exp(-Q^2u^2)$ is the Debye-Waller factor, and u^2 is the mean-square displacement of the atoms from their equilibrium positions in the direction of $\mathbf{Q}$. The population factor $N_j=[\exp(h\nu_j/k_BT)-1]^{-1}$ is used for phonon annihilation (neutron energy gain), and N_j+1 for phonon creation (neutron energy loss).

Lead was chosen as the material for study for several reasons.

1. It has good nuclear and chemical properties and large single crystals are available.

2. The Debye temperature is very small (about 1/7 of the melting temperature), and hence there is a large region of temperature in which anharmonic effects can be studied.

3. The entire temperature range in which the crystal exists is easily accessible, and the melting temperature is conveniently located for study of both crystalline and liquid[12] lead.

4. The lattice vibrations in lead are almost entirely determined by the strictly metallic forces. This is not true of all metals, for example in copper the overlap forces between ions play a crucial role.[13,14]

5. Lead is a superconductor with a comparatively high transition temperature. It is therefore a good material in which to study any possible effects of superconductivity on the lattice vibrations.[4,8] The high transition temperature and other superconducting and electrical properties indicate that electron-phonon interaction is especially large in lead, and this made it an interesting material for study at higher temperatures. In particular it seemed a suitable material in which to look for the Kohn effect.[7,3]

It has one disadvantage as a material for study in that the frequencies are inconveniently small, without however being small enough so that much advantage can be taken of the beryllium cutoff for order elimination, etc.[5] Nevertheless, it has been possible to measure the frequencies to an accuracy of 1 to 2%, and this accuracy has proved adequate to delineate the qualitative features of the lattice dynamics.

II. THE EXPERIMENTS

1. Experimental Details

Two of the lead single crystals[2] were in the form of spheres cut from large ingots which were grown from the melt by the Bridgeman method in graphite crucibles in a vertical furnace. Specimen A was about 6 cm in diameter after a light etch in dilute nitric acid. Specimen B was about 5 cm in diameter after a very heavy etch in dilute nitric acid. Both specimens showed lineage structure in the characteristic single-crystal sheen of the etched surface. The rocking curves of specimen A were about 2 deg full width at half-maximum, and those of specimen B were 1.3 deg. The third specimen (C) was a rectangular crystal about 1.6 cm×3.5 cm ×5 cm which was cut from the interior of an ingot. The exterior of the ingot showed lineage structure as usual, but an irregularly shaped region in the interior was unusually good, with a rocking curve whose width was only a few minutes of arc. This crystal was used for the new measurements described in this paper. The crystals were aligned *in situ* using neutrons. The alignment was probably good to a few minutes of arc.

The experiments were carried out using the triple axis crystal spectrometer[5] at the N.R.U. reactor. (Some preliminary measurements using the rotating crystal spectrometer[5] were described in reference 1.) A schematic diagram of the apparatus is shown in Fig. 1. Neutrons from the reactor are Bragg reflected by the monochromating crystal $X1$ through an angle $2\theta_M$, thus determining E_0 and $|\mathbf{k}_0|$. The monoenergetic neutrons incident on the specimen crystal S are observed at an angle of scattering ϕ by the analyzing spectrometer. The scattered neutrons are Bragg reflected by the analyzing crystal $X2$ through the angle $2\theta_A$, thus determining E' and $|\mathbf{k}'|$. The specimen crystal S is oriented with a principal plane in the plane of the spectrometers, and aligned in the plane with respect to the neutron beam ($\mathbf{k}_0$) by changing the angle ψ. The four angles $2\theta_M$, $2\theta_A$, ϕ and ψ are all continuously variable and electrically controlled.

The measurements could be carried out in the

[11] R. Weinstock, Phys. Rev. **65**, 1 (1944).
[12] B. N. Brockhouse and N. K. Pope, Phys. Rev. Letters **3**, 259 (1959).
[13] N. F. Mott and H. Jones, *The Theory of the Properties of Metals and Alloys* (Oxford University Press, New York, 1936), Chap. 4.
[14] H. C. White, Phys. Rev. **112**, 1092 (1958).

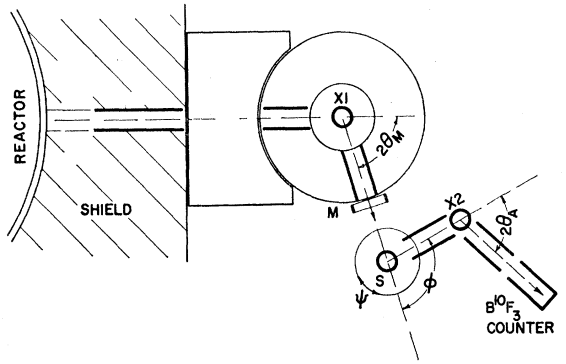

FIG. 1. Schematic drawing of the apparatus.

conventional way with a fixed incoming energy, E_0, by measuring the energy distribution of the outgoing neutrons by varying the angle $2\theta_A$. In this method the frequency for a desired $\mathbf{q}$ is obtained by repeated experiments using successive approximations.

A more sophisticated method, called the "constant momentum transfer method" or "constant $\mathbf{Q}$" method,[5] is generally employed. With a fixed incoming energy, the angle of scattering ϕ and crystal orientation ψ are varied nonlinearly in step with the angle $2\theta_A$ of the analyzing spectrometer (and thus with $|\mathbf{k}'|$), in such a way as to keep the vector $\mathbf{Q}=\mathbf{k}_0-\mathbf{k}'$ constant. Thus by Eq. (2a) any neutron group which appears in the energy distribution gives the frequency of a phonon with wave vector $\mathbf{q}$ in the reduced zone. The increments in the angles required to accomplish this are calculated on a digital computer, and the instructions transmitted to the spectrometer by means of a punched paper tape.[5] Figure 2 shows the limits of a typical experiment designed to determine the frequency of the longitudinal phonon at the point $(a/2\pi)\mathbf{Q}=(0,0,3)$, that is, with $\mathbf{q}$ at the zone boundary in the $[00\zeta]$ direction[15] of the reduced zone.

For technical reasons it is often desirable to use another mode of operation in which $2\theta_A$ (and therefore $|\mathbf{k}'|$) is kept fixed and the incoming energy varied by means of $2\theta_M$. In the constant $\mathbf{Q}$ method ϕ and ψ are then changed nonlinearly in step with $2\theta_M$, in such a way as to keep $\mathbf{Q}$ fixed. The limits of a typical experiment designed to determine the frequency of the longitudinal phonon at the point $a\mathbf{Q}/2\pi=(3/2,3/2,3/2)$, that is at the zone boundary of the $[\zeta\zeta\zeta]$ direction in the reduced zone, are shown in Fig. 3.

Measurements were made along the symmetric lines $[\zeta 00]$, $[\zeta\zeta\zeta]$, $[\zeta\zeta 0]$, and $[\zeta 10]$ of the reduced zone at temperatures within ten degrees of 100°K. (Measurements were also made along the zone boundary in a {110} plane, a nonsymmetric direction.)

[15] This would ordinarily be termed the [001] direction, but the present notation is used since we will also discuss lines in reciprocal space in which one component or more is constant, with others varying.

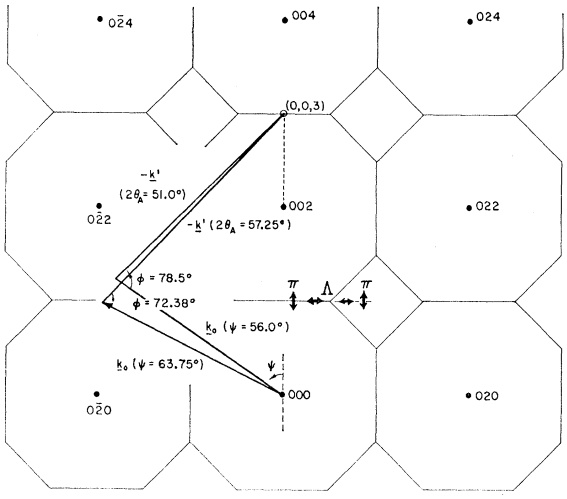

FIG. 2. The (100) plane of the reciprocal lattice with a typical "constant $\mathbf{Q}$" experiment designed to measure the frequency of the longitudinal phonon at the point (0,0,3), i.e., at the point X in the reduced zone. The double-headed arrows $\mathbf{\Lambda}$, $\boldsymbol{\pi}$ show the directions of the polarizations along the line $[0\zeta 1]$. The third polarization vector is normal to the (100) plane, and has the same $\nu(\mathbf{q})$ relation as $\boldsymbol{\pi}$ but shifted in phase.

Using the method of successive approximations, sometimes with the associated techniques[5] for keeping $\mathbf{q}$ in the correct direction, measurements were made on specimens A and B in $[\zeta 00]$, $[\zeta\zeta\zeta]$, and $[\zeta\zeta 0]$ directions of a {110} plane and also along the zone boundary. The (111) and (200) planes of aluminium crystals were variously used as the monochromator and analyzer, and wavelengths of 1.91 Å and 2.26 Å were employed. Details and typical neutron groups were presented in reference 2.

Using the constant $\mathbf{Q}$ method with fixed incoming energy, measurements were made in $[\zeta 00]$, $[\zeta\zeta 0]$, and $[\zeta 10]$ directions in a {100} plane of specimen B. The Al (111) monochromator was set to a wavelength of 2.26 Å, and the Al (200) analyzer was generally employed. Figure 2 shows the (100) plane of the reciprocal lattice with the initial and final vector diagram for a typical experiment. Typical neutron groups were shown in reference 2.

Using the constant $\mathbf{Q}$ method with fixed analyzer energy, measurements were made in $[\zeta 00]$, $[\zeta\zeta 0]$, and $[\zeta\zeta\zeta]$ directions of the reduced zone, in a {110} plane of specimen C. Lines studied in reciprocal space are shown in Fig. 3 as dashed lines. They were selected to afford maximum discrimination between longitudinal and transverse modes, through the factor $(\mathbf{Q}\cdot\boldsymbol{\xi})^2$ in Eq. (3). The limits of the vector diagram [Eq. (2a)] for a typical experiment are also shown in Fig. 3. A typical series of neutron groups is shown in Fig. 4. The number of counts accumulated during a preset number of monitor counts[16] is plotted as a function of

[16] The monitor is a thin fission counter located in the monoenergetic beam (indicated as M in Fig. 1).

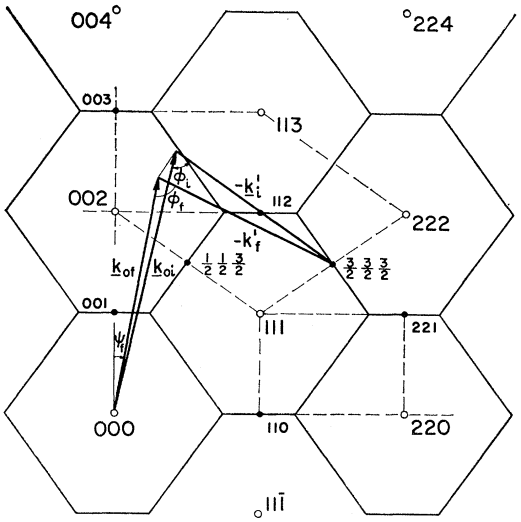

FIG. 3. The $(1\bar{1}0)$ plane of the reciprocal lattice with a "constant **Q**" experiment (showing the initial and final vector diagrams) designed to measure the frequency of the longitudinal phonon at the point (3/2,3/2,3/2), i.e., at the point L in the reduced zone. Measurements were made along the dashed lines in reciprocal space.

the frequency calculated from Eq. (2b). In these (and most other) experiments the (1,1,1) aluminum analyzer was fixed with $2\theta_A=67°$, and thus with $E'=12.28\times10^{-3}$ eV [$\lambda'=2.58$ Å]. For the neutron groups at the bottom of the figure, the variables E_0, ϕ, ψ took on values shown in the subsidiary abscissa scales. This group was taken at $(a\mathbf{Q}/2\pi)=(1.5,1.5,1.5)$; the corresponding vector diagram is shown in Fig. 3. Other neutron groups are shown later.

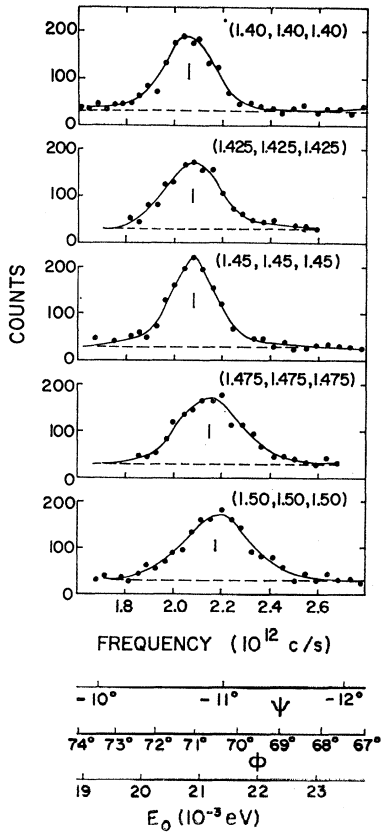

FIG. 4. A set of "constant **Q**" experiments made at points between (1.4,1.4,1.4) and (1.5,1.5,1.5) in reciprocal space. Auxiliary scales for the three experimental variables E_0, ϕ, and ψ are shown at the bottom for the (1.5,1.5,1.5) experiment, also shown in Fig. 3.

2. The Experimental Dispersion Curve

The centers of the neutron groups obtained in the different experiments were used to define values of ν and $\mathbf{q}$ by Eq. (2). The composite results are shown in Fig. 5, the results with conventional methods as open circles, and the results with the constant **Q** method in a {100} plane as closed circles. The newer results with the constant **Q** method in a {110} plane are shown as crosses. The curves are plotted in such a way as to display their inter-relationship.

It is believed that the scatter of the points is a fair measure of the errors in the dispersion curves of Fig. 5, especially where several independent experimental arrangements were involved. The slopes of the dispersion curves at $\mathbf{q}=0$ are indicated in Fig. 5, as calculated from recent ultrasonic measurements of Waldorf.[17]

The effects of resolution in reciprocal space are almost certainly small except for phonons of small $\mathbf{q}$, and possibly for phonons near the point (1,0,0) of the reduced zone. The resolution varied somewhat from experiment to experiment. In the horizontal plane it was approximately given by $\delta_H(qa/2\pi)\simeq\pm0.03$, as estimated from the resolution elements and from the widths of the observed groups, and thus it was of negligible importance. The resolution normal to the plane of the spectrometer was of greater importance. The vertical divergence of the collimating slits was about $\pm1\frac{1}{2}$ deg for k' and about $\pm0.6°$ for k_0. The resolution normal to the plane of the spectrometer is therefore about $\delta_V(qa/2\pi)\simeq\pm0.06$. For phonons at a nominal reduced wave number $(qa/2\pi)=0.2$ the correction would change the reduced wave vector by $\delta(qa/2\pi)\approx0.01$, i.e., by 5%, and would ordinarily be negligible for reduced wave vectors $\gtrsim0.4$. Actually the correction depends strongly on the details of the dispersion surfaces $\nu(\mathbf{q})$ in the vicinity of $\mathbf{q}$. Because of this we have not made any corrections for resolution to our measurements.

Because of the frequency dependence of the cross section, Eq. (3), a correction should be applied for energy resolution. The order of magnitude of this correction can be estimated as

$$\Delta\nu\sim\tfrac{1}{4}W^2/\nu_M,$$

where W is the full width at half-maximum of the neutron group in units of frequency, and ν_M is the mean frequency of the group. The constant $(\sim1/4)$

[17] D. L. Waldorf, Bull. Am. Phys. Soc. **5**, 170 (1960).

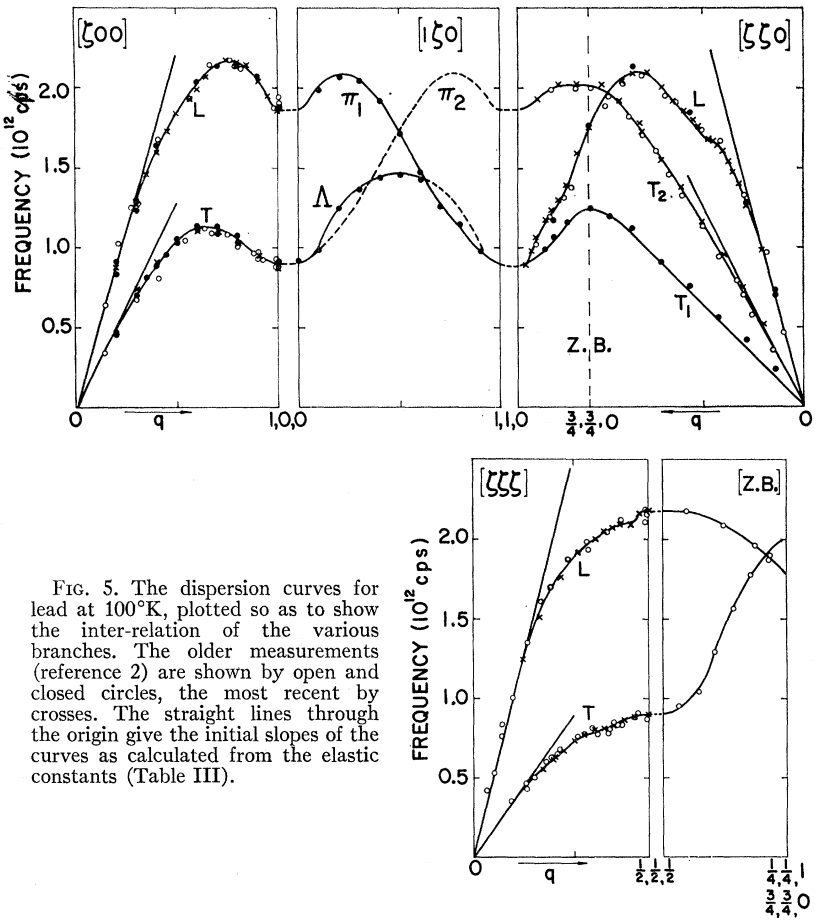

FIG. 5. The dispersion curves for lead at 100°K, plotted so as to show the inter-relation of the various branches. The older measurements (reference 2) are shown by open and closed circles, the most recent by crosses. The straight lines through the origin give the initial slopes of the curves as calculated from the elastic constants (Table III).

actually depends on the shape of the peak and on the ratio $h\nu/k_BT$. Typically this correction turned out to be about 0.5%, and was ignored. For some especially broad groups the correction was applied and brought the frequencies into good agreement with narrow groups at the same **q**. Most of the broad groups were omitted from the final data compilation nevertheless.

Values of the frequencies for the three symmetric directions, with estimates of over-all "probable" errors, are given in Tables I and II. The errors contain allowance for calibration and other determinate errors, and hence cannot be expected to be random. Values for the [ζ10] direction, and for the zone boundary in the (110) plane, are possibly less accurate since only one set of

TABLE I. Frequencies (units 10^{12} cps) of the lattice vibrations in lead at 100°K which propagate in the [ζ00] and [ζζζ] directions.

[ζ00]			[ζζζ]			
	T	L		T		L
$aq/2\pi$	ν	ν	$aq/2\pi$	ν	$aq/2\pi$	ν
0.20	0.47 ±0.04	0.87±0.03	0.19	0.35 ±0.04	0.143	0.82 ±0.05
0.30	0.73 ±0.03	1.27±0.03	0.26	0.44 ±0.03	0.25	1.24 ±0.04
0.40	0.90 ±0.02	1.61±0.03	0.35	0.55 ±0.03	0.332	1.51 ±0.04
0.45	0.96 ±0.03	1.71±0.04	0.40	0.61 ±0.02	0.433	1.76 ±0.03
0.50	1.04 ±0.02	1.83±0.04	0.45	0.66 ±0.02	0.519	1.91 ±0.03
0.55		1.91±0.03	0.50	0.73 ±0.02	0.563	1.97 ±0.03
0.60	1.115±0.02	2.00±0.03	0.55	0.77 ±0.02	0.606	2.00 ±0.03
0.65		2.07±0.03	0.60	0.79 ±0.02	0.649	2.05 ±0.03
0.70	1.10 ±0.03	2.14±0.04	0.65	0.805±0.02	0.693	2.085±0.02
0.75		2.16±0.02	0.70	0.835±0.02	0.736	2.09 ±0.02
0.80	1.03 ±0.03	2.15±0.02	0.75	0.86 ±0.02	0.779	2.08 ±0.03
0.85		2.14±0.02	0.80	0.88 ±0.02	0.823	2.16 ±0.03
0.90	0.95 ±0.02	2.05±0.03	0.867	0.89 ±0.02	0.867	2.185±0.02
0.95		1.94±0.04				
1.00	0.89 ±0.02	1.86±0.03				

TABLE II. Frequencies (units 10^{12} cps) of the lattice vibrations in lead at 100°K which propagate in the [ζζ0] direction. The zone boundary is at $aq/2\pi=1.061$.

Longitudinal				T_2; $\xi=(0,0,1)$		T_1; $\xi=(1/\sqrt{2})(1,\bar{1},0)$	
$aq/2\pi$	ν	$aq/2\pi$	ν	$aq/2\pi$	ν	$aq/2\pi$	ν
0.212	0.99 ±0.04	0.70	2.01 ±0.02	0.20	0.53±0.03	0.141	0.21±0.03
0.284	1.26 ±0.04	0.778	2.10 ±0.02	0.30	0.75±0.03	0.283	0.41±0.03
0.325	1.40 ±0.04	0.85	2.09 ±0.02	0.40	0.95±0.03	0.424	0.56±0.03
0.35	1.48 ±0.03	0.90	2.04 ±0.03	0.50	1.17±0.03	0.566	0.76±0.03
0.375	1.545±0.02	0.99	1.925±0.04	0.60	1.37±0.03	0.707	0.91±0.03
0.40	1.605±0.02	1.061	1.75 ±0.04	0.70	1.57±0.03	0.848	1.12±0.03
0.425	1.64 ±0.02	1.132	1.54 ±0.04	0.814	1.78±0.03	0.959	1.20±0.03
0.45	1.665±0.02	1.173	1.39 ±0.03	0.914	1.92±0.04	1.056	1.25±0.03
0.475	1.675±0.03	1.215	1.30 ±0.03	1.00	2.02±0.03	1.17	1.15±0.03
0.50	1.715±0.02	1.244	1.24 ±0.03	1.12	2.02±0.03	1.241	1.06±0.04
0.525	1.76 ±0.02	1.272	1.185±0.03	1.214	2.02±0.03	1.281	0.96±0.04
0.55	1.795±0.02	1.314	1.07 ±0.03	1.314	1.93±0.04	1.414	(0.89±0.02)
0.60	1.85 ±0.02	1.373	0.885±0.03	1.414	(1.86±0.03)		
0.65	1.92 ±0.02	1.414	(0.89 ±0.02)				

measurements for each was made. The values for the [ζ10] direction also suffer from possible error arising from the possible existence of anomalous neutron groups as discussed in the next section.

3. Anomalous Neutron Groups

The intensities of the groups are proportional to the factor $(\mathbf{Q}\cdot\xi_j)^2$ in Eq. (3). Normally, measurements were made in positions in the reciprocal lattice for which this factor had close to its maximum value Q^2. On the one hand, this made the intensities easily measurable, and on the other hand, it should have made it possible to identify the branch to which a strong phonon belonged. Thus, for example, only longitudinal phonons should be observed along the line [00Q] since for transverse phonons the factor $(\mathbf{Q}\cdot\xi)^2=0$.

Nevertheless we observed, in crystals A and B, several neutron groups which gave values of ν and $\mathbf{q}$ in reasonable agreement with the $\nu(\mathbf{q})$ curve for the [00ζ] T branch at $\mathbf{Q}$'s from $(2\pi/a)(0,0,1.6)$ to $(2\pi/a)(0,0,2.5)$ for which only [00ζ] L phonons should be observed. A typical pattern, for $(a/2\pi)\mathbf{Q}=(0,0,2.3)$, is shown in Fig. 6(a). A strong group appears at a frequency corresponding to the transverse mode at the point (0,0,0.3) in the reduced zone, though from Eq. (3) only the longitudinal mode should appear. The temperature variation of the intensities of these anomalous neutron groups was studied in a limited way, without definitive results. Sometimes the intensities (for groups in energy gain) increased strongly with temperature, as with phonons, and sometimes they seemed relatively independent of the temperature.

We ascribe[2] these groups to a double scattering process, in which a one phonon group of neutrons undergoes a second (Bragg) scattering, or vice versa. Then, if $\mathbf{k}'$ is the neutron wave vector after the first scattering and $\mathbf{k}''$ after the second scattering,

$$\mathbf{k}_0-\mathbf{k}'=2\pi\tau_1-\mathbf{q},\quad \mathbf{k}'-\mathbf{k}''=2\pi\tau_2.$$

Adding, we have

$$\mathbf{k}_0-\mathbf{k}''=2\pi(\tau_1+\tau_2)-\mathbf{q}=2\pi\tau_3-\mathbf{q},$$

since the sum of two reciprocal lattice vectors is itself a reciprocal lattice vector. Thus, the one phonon-elastic double-scattering process still give groups in the correct positions but the intensities need no longer satisfy the one-phonon theoretical expression, either as to polarization dependence or as to temperature dependence.

With the better specimen C the anomalous neutron groups were weak, if present at all. A typical pattern [Fig. 6(b)] shows no anomalous group, though it does show extra scattering at low frequencies, probably from multiple-phonon and multiple-event inelastic scattering. This behavior agrees with expectations, since both the probability of the one phonon-elastic double scattering process, and its intensity, are smaller for a relatively perfect crystal than for an imperfect crystal.

These anomalous neutron groups can only be clearly demonstrated to exist when the different branches for the wave vector concerned are widely separated in frequency. There is no reason to suppose that they do not also exist when the frequencies are close together. In this case their existence will introduce error into the frequency determination since the position of the mean of the neutron groups will be altered.

Consideration of the probability of occurrence of the double scattering leads to the conclusion that the process may be the rule rather than the exception for large crystals which are efficient Bragg scatterers (i.e., efficient monochromators). Thus, the crystals should be as perfect as possible, particularly if the intensities are to be used[5] for branch identification or in the analysis, or if the branches are close together in frequency.

III. BORN-VON KÁRMÁN ANALYSIS

We first analyze the experimental results in terms of the familiar Born-von Kármán theory of lattice dy-

namics. For convenience we consider $\mathbf{q}$ in a symmetric direction in crystal, a direction which is the intersection of two or more mirror planes. The polarization vector, ξ_j, the direction of vibration of the single atom in the unit cell, can then only be normal to or parallel to the wave vector $\mathbf{q}$.

For the degenerate transverse modes in the $[\zeta 00]$ and $[\zeta\zeta\zeta]$ directions, ξ may lie in any direction normal to $\mathbf{q}$. In the $[\zeta\zeta 0]$ direction, the two transverse modes are distinct with ξ lying in the $[1\bar{1}0]$ and $[001]$ directions for T_1 and T_2, respectively.

In the Born-von Kármán theory restoring forces between atoms depend linearly on the relative displacements of the atoms. The equations of motion of the lth atom (in the lth primitive unit cell) *for a particular mode in a particular symmetric direction* is

$$M\ddot{u}_{\alpha l}=-\sum_{l'}\Phi_{\alpha\alpha}(l,l')u_{\alpha l'}, \tag{4}$$

where $u_{\alpha l}$ is the displacement of atom l in the particular direction α (of polarization) considered, and M is the mass of the atoms. $\Phi_{\alpha\alpha}(l,l')$ represents the restoring force exerted on atom l in the direction α, when atom l' is moved a unit distance also in direction α. The summation includes the term $l=l'$, and $\sum_l\Phi_{\alpha\alpha}(l,l')=0$ in order that the crystal may be stable under uniform translation. Let the solution of (4) have the form of a traveling wave:

$$u_{\alpha l'}=U_\alpha\exp(i\mathbf{q}\cdot\mathbf{R}_l)\exp(i\mathbf{q}\cdot\mathbf{R}_{ll'}-i\omega t), \tag{5}$$

where $\mathbf{R}_l$ is the vector distance of the lth atom from the origin and $\mathbf{R}_{ll'}$ is the vector distance of the l'th atom from the lth atom. Substituting Eq. (5) in Eq. (4) we obtain

$$M\omega^2=\sum_{l'}\Phi_{\alpha\alpha}(l,l')\exp(i\mathbf{q}\cdot\mathbf{R}_{ll'}). \tag{6}$$

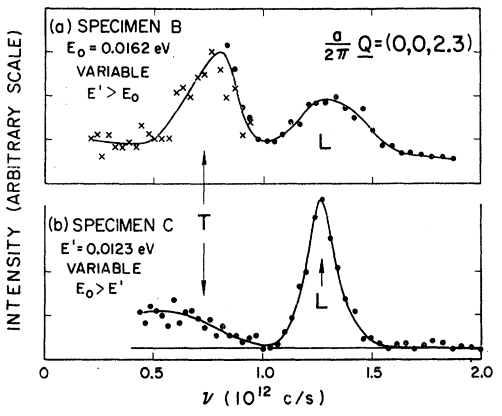

FIG. 6. Constant **Q** experiments at the point (0,0,2.3), $\mathbf{q}=(2\pi/a)[0,0,0.3]$, at which only the longitudinal mode should appear. An anomalous neutron group with a frequency about that of the transverse mode was found with specimen B. The measurements shown as crosses were made later at a lower counting time per point than were the principal measurements.

TABLE III. The elastic constants for the symmetry directions in a cubic crystal and the parameter B. The three basic constants of lead at 100°K (reference 17) are $c_{11}=5.437$, $c_{12}=4.505$, $c_{44}=1.819$, all in units of 10^{11} dyn/cm^2.

Branch	Elastic constant c_i	B
$[\zeta 00]$ T	c_{44}	1
$[\zeta 00]$ L	c_{11}	1
$[\zeta\zeta\zeta]$ T	$(c_{11}-c_{12}+c_{44})/3$	3/4
$[\zeta\zeta\zeta]$ L	$(c_{11}+2c_{12}+4c_{44})/3$	3/4
$[\zeta\zeta 0]$ T_1	$(c_{11}-c_{12})/2$	2
$[\zeta\zeta 0]$ T_2	c_{44}	2
$[\zeta\zeta 0]$ L	$(c_{11}+c_{12}+2c_{44})/2$	2

This can be written as

$$M\omega^2=\sum_{n=1}^{N}\Phi_n[1-\cos(n\pi q/q_M)], \tag{7}$$

where q_M is half the distance to the nearest reciprocal lattice point in the direction of $\mathbf{q}$, $q=|\mathbf{q}|$ and Φ_n is a linear combination of $\Phi_{\alpha\alpha}(l,l')$ for which the phase $\mathbf{q}\cdot\mathbf{R}_{ll'}$ is a constant. Φ_n effectively represents a force between a particular atom and the (two) planes of atoms normal to $\mathbf{q}$ and n planes away. The sum is taken to a number of terms N such that $\Phi_n=0$ for $n>N$.

Following Foreman and Lomer,[18] we used Eq. (7) to determine the range of the interatomic forces in lead from the dispersion curves. (See also reference 2). Appropriately weighted frequencies of phonons, of the particular branch and direction considered, were fitted by least squares to an expression of the form of Eq. (7) using different numbers of terms N in the series. We included in the fits the appropriate elastic constants c_i, using values interpolated from measurements of Waldorf,[17] and the equation

$$\pi^2Bac_i=\sum_{n=1}^{N}\tfrac{1}{2}n^2\Phi_n. \tag{8}$$

(The constant B and the elastic constant c_i depend on the branch considered, and are listed, together with the values of the elastic constants, in Table III.) The values of Φ_n for two branches obtained in the fits are shown in Fig. 7, plotted as a function of the number of terms used in the fits. It will be observed that the values of the coefficients Φ_n are substantially independent of the number of terms used in the fits.

The rms deviations (Δ_N) of a single experimental value of $M\omega^2$ from the fitted curve was also computed, and $\Delta_N/10$ is also plotted against N in Fig. 7. It decreases steadily to an approximately stable value which corresponds very nicely to the estimated error of 1 to 2% in frequency. (The stable value actually

[18] A. J. E. Foreman and W. M. Lomer, Proc. Phys. Soc. (London) **B70**, 1143 (1957).

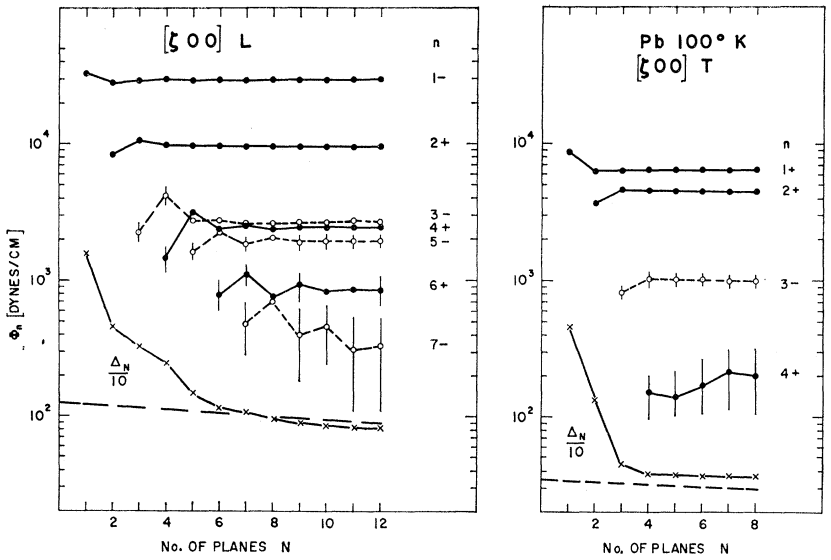

FIG. 7. The interplanar force constants for the longitudinal and transverse branches in the [ζ00] direction plotted as functions of the number of planes used in the fits. The plane number and the sign of the force constant are at the right in each figure. The rms deviation (÷10) of the fitted curve from the measured values of $M\omega^2$ is also plotted for each branch.

decreases slowly with N because of the finite number of measurements used in the fits.)

From the behavior of both the Φ_n and Δ_N in Fig. 7 it appears that at least three and probably four planes are needed to fit the [ζ00] T branch, and that at least six planes are needed to fit the [ζ00] L branch. For the [ζ00] direction four planes correspond to interactions out to at least eighth neighbor atoms, and six planes out to at least seventeenth neighbors. In Fig. 8 the values of $M\omega^2$ for the [ζ00] L branch are shown, together with the Fourier composition and the fits for $N=5$ and 12, plotted against the reduced wave vector. In Fig. 9 Φ_n is plotted against n, effectively the distance between interacting planes of atoms, for the [ζ00] L branch. The force between planes is seen to oscillate at large distances. This oscillation is connected with the sharp drop in frequency of the [ζ00] L branch near the zone boundary. The same behavior, though less marked, can be seen in some of the other branches in Table IV.

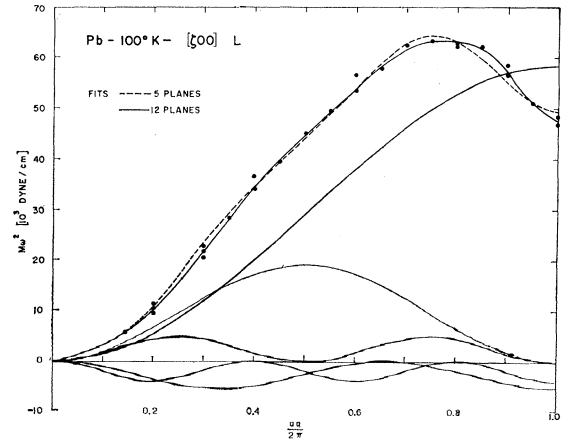

FIG. 8. Values of $M\omega^2$ for the longitudinal branch in the [ζ00] L direction plotted against the reduced wave vector. The fitted curves with 12 planes (good fit) and with 5 planes (possibly a fit) are shown. The first five Fourier components are also plotted.

If the elastic constants were omitted from the fits the results obtained were essentially unchanged. Conversely, it was not possible to deduce unambiguous values of the elastic constants from the neutron measurements. The smallest values of N at which satisfactory fits were obtained usually yielded values of the elastic constants in agreement with experiment, at larger values of N the calculated elastic constants fluctuated widely. This behavior comes about from the excessive sensitivity of the elastic constants to the high Fourier components [see Eq. (8)].

Measurements along the line [ζ10] were also fitted to an expression of the form of Eq. (7) with an additional constant term Φ_0. The results are given in Table IV. From the symmetry of the reciprocal lattice (Fig. 2) it is easily seen that the polarization vectors must lie along one of the three coordinate axes, as shown by the arrows denoted Λ and π. Thus the problem is a linear one since the three modes are separable. The Φ_n are not interplanar forces, however, but merely linear combinations of the interatomic force constants since the atoms in any one plane have different phases.

The $\Phi_{\alpha\alpha}(l,l')$ are interatomic force constants of the usual description, but their number can be greatly reduced by application of the symmetry requirements of the crystal using standard methods.[10] For each class of neighbor there are at most six independent force constants, which may be further reduced by symmetry. Thus, for the twelve first neighbors at positions of the

type $\frac{1}{2}a(1,1,0)$ there are three force constants

$$\alpha_1 \equiv \Phi_{xx}(\tfrac{1}{2}a(1,1,0)) = \Phi_{yy}(\tfrac{1}{2}a(110)) \equiv \langle x,x\rangle,$$
$$\beta_1 \equiv \Phi_{zz}(\tfrac{1}{2}a(1,1,0)) \equiv \langle z,z\rangle,$$
$$\gamma_1 \equiv \Phi_{xy}(\tfrac{1}{2}a(1,1,0)) \equiv \langle x,y\rangle.$$

The composition of the planar coefficients Φ_n in terms of these constants is given in Table V (to fifth neighbors). Thus, for the $[\zeta 00]$ T branch

$$M\omega^2 = (4\alpha_1+4\beta_1+8\alpha_3+8\beta_3+4\alpha_5+4\gamma_5)(1-\cos\pi\zeta) + (2\beta_2+8\beta_3+4\alpha_4+4\beta_4)(1-\cos 2\pi\zeta) + (4\beta_5+4\gamma_5)(1-\cos 3\pi\zeta).$$

We tried to solve for atomic force constants by fitting the force constants by least squares to the measurements of Table IV, cutting off at fifth neighbors. The results were of no use because the errors introduced by cutting off were larger than all except the first neighbor constants. (The only positive result is that $\alpha_1 \sim 4\times 10^3$ dyn/cm and β_1 is negative, $\sim -2\times 10^3$ dyn/cm). It does not appear possible to increase the number of interacting neighbors sufficiently to allow a meaningful fit to be carried out. The amount of "orthogonal" information in the measurements so far carried out is sufficient only to allow fitting out to eighth neighbors,[2,18] regardless of the accuracy of the measurements. Even so, separate values of all the force constants could not be obtained. For example, γ_1 could not be separated from δ_5. To go further, new measurements would be required in nonsymmetry directions with resulting difficulties[5] in carrying out the fits.

To sum up, the results show that the interatomic forces in lead are of long range and sometimes of alternating sign. Because of the long range it is not possible to obtain a detailed description of the force constants in the Born-von Kármán theory.

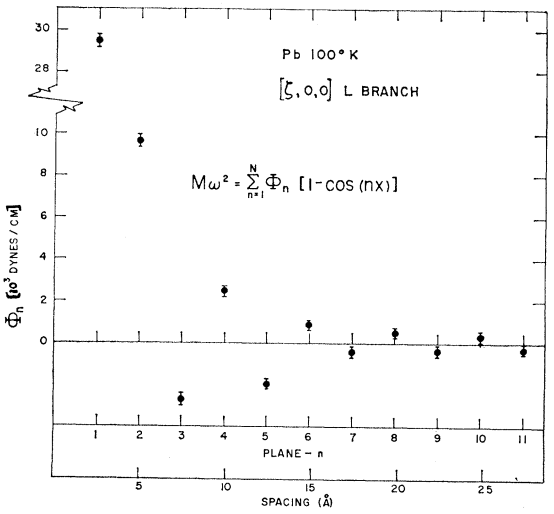

FIG. 9. The interplanar force constants for the $[\zeta 00]$ L branch.

IV. INFLUENCE OF THE FERMI SURFACE ON LATTICE VIBRATIONS

1. Experiments

On theoretical grounds, Kohn[7] has proposed that there exist lines through reciprocal space at which the dispersion surface of the lattice vibrations have infinite slopes. The positions of these anomalies are related to the Fermi surface, and the infinite slopes to the sharpness of the Fermi surface. For a spherical Fermi surface, as for free electrons, the anomalies occur at positions in reciprocal space given by the equation:

$$2K_F = |2\pi\tau + \mathbf{q}|, \tag{9}$$

where K_F is the Fermi radius. Computations[19,20] of the effect have been made for ideally free electrons; for

TABLE IV. Interplanar force constants Φ_n for lead at 100°K in units of 10^3 dyn/cm.[a]

	Φ_0	Φ_1	Φ_2	Φ_3	Φ_4	Φ_5	Φ_6	Φ_7	Φ_8	
$[\zeta 00]$ T	···	6.50	4.54	−1.0	0.20	0.09	0.01	−0.10	0.03	±0.10
$[\zeta 00]$ L	···	29.45	9.70	−2.60	2.45	−1.95	0.85	−0.35	0.55	±0.25
$[\zeta\zeta\zeta]$ T	···	5.20	0.30	0.05	−0.10	0.19	−0.05	−0.05	0.10	±0.10
$[\zeta\zeta\zeta]$ L	···	29.6	5.8	1.4	−0.4	0.4	0.1	0.6	−0.3	±0.45
$[\zeta\zeta 0]$ L	···	7.6	24.6	−3.2	2.65	2.0	−0.05	−0.8	−0.2	±0.17
$[\zeta\zeta 0]$ T_2	···	28.6	4.5	−3.8	2.0	−0.3	0.4	−0.35	0.15	±0.25
$[\zeta\zeta 0]$ T_1	···	8.95	3.05	−3.0	1.85	−0.60	0.05	−0.01	−0.02	±0.15
$[\zeta 10]$ Λ	10.7	···	8.9	···	2.0	···	0.5	···		±0.2
$[\zeta 10]$ Π	44.5	−23.0	5.0	4.7	2.8	0.6	1.5	1.0		±1.0

[a] Notes: 1. Coefficients marked ··· are zero by symmetry. 2. The vertical lines mark off values of Φ_n contributed to by 2 neighbors (——), 5 neighbors (— — —), and 8 neighbors (– – – –). 3. The errors given are approximate errors in the force constants incurred in fitting the experimental data. For absolute errors they should be increased by a factor of perhaps two.

[19] T. Toya, Jour. Research Inst. Catalysis, Hokkaido Univ. **6**, 161 (1958).
[20] E. J. Woll, Jr., and S. J. Nettel, Bull. Am. Phys. Soc. **6**, 144 (1961); E. J. Woll, Jr., and W. Kohn, Phys. Rev. **126**, 1693 (1962).

TABLE V. Interatomic force constant composition of interplanar force constants Φ_n for symmetry branches in a face-centered cubic crystal.

Position of atom →		$\frac{1}{2}a(1,1,0)$			$\frac{1}{2}a(2,0,0)$		$\frac{1}{2}a(2,1,1)$				$\frac{1}{2}a(2,2,0)$			$\frac{1}{2}a(3,1,0)$			
Branch	n	α_1 $\langle x,x\rangle$	β_1 $\langle z,z\rangle$	γ_1 $\langle x,y\rangle$	α_2 $\langle x,x\rangle$	β_2 $\langle y,y\rangle$	α_3 $\langle x,x\rangle$	β_3 $\langle y,y\rangle$	γ_3 $\langle y,z\rangle$	δ_3 $\langle x,y\rangle$	α_4 $\langle x,x\rangle$	β_4 $\langle z,z\rangle$	γ_4 $\langle x,y\rangle$	α_5 $\langle x,x\rangle$	β_5 $\langle y,y\rangle$	γ_5 $\langle z,z\rangle$	δ_5 $\langle x,y\rangle$
[ζ00] T	1	4	4				8	8						4		4	
	2					2		8			4	4					
	3														4	4	
[ζ00] L	1	8						16							8		
	2				2		8				8						
	3													8			
[ζζζ] T	1	4	2	−2	2	4	4	8	4					4	4	4	4
	2						2	4	−2	−4	4	2	−2	4	4	4	−4
[ζζζ] L	1	4	2	4	2	4	4	8	−8					4	4	4	−8
	2						2	4	4	8	4	2	4	4	4	4	8
[ζζ0] T_2	1	8						8						8			
	2		2			4	4				8					4	
	3							8							8		
	4											2				4	
[ζζ0] T_1	1	4	4				4	4		8					4	4	
	2	2		−2	2	2		4	−4		4	4		2	2		4
	3						4	4		−8				4		4	
	4										2		−2	2	2		−4
[ζζ0] L	1	4	4				4	4		−8					4	4	
	2	2		2	2	2		4	4		4	4		2	2		−4
	3						4	4		8				4		4	
	4										2		2	2	2		4
[ζ00] Λ	0	8	8				16	16						8	8	16	
	2				2		−8				8						
[ζ10] Π	0	16						32						16	16		
	1	−4	4				8	−8						−4		4	
	2					2		−8			4	4					
	3														−4	4	

this case the anomalies turn out to be too small for observation at present.

Nevertheless we believe that the anomalies visibly present in the dispersion curves of Fig. 5 are, in fact, Kohn anomalies. In this section we present the experimental evidence for the reality of the observed anomalies, and discuss their relation with the Fermi surface. In the following section their unexpectedly large magnitude will be discussed from a theoretical point of view.

In an earlier report[3] we discussed the anomalies on the basis of the free electron model with a spherical Fermi surface; here we will proceed immediately to consider the real metal with a real Fermi surface. Figure 10 shows the cross section in the $(1\bar{1}0)$ plane of reciprocal space of the Fermi surface of lead in the extended zone scheme.[21] According to Gold[22] the Fermi surface of lead is only moderately distorted at the intersections of the free electron sphere with Bragg reflecting planes (as shown in Fig. 10). The Fermi surface of Fig. 10 satisfies the experiments of Gold on the de Haas-van Alphen effect, as well as the results of this paper. The anomalies of Kohn occur at wave vectors through which abnormally large numbers of electrons can be elastically scattered. Two such transition wave vectors are indicated in Fig. 10 by the solid lines (F) and the dashed line (G). Transition F is found to correspond very closely to an anomaly in the longitudinal branch in the [ζζζ] direction, and transition G to an anomaly in the [ζζ0] L branch.

Figure 11 shows the accumulated results for the [ζζζ] L branch. Measurements were made along the line $\mathbf{Q}=(2\pi/a)(h,h,h)$ in reciprocal space in two regions: (A) from (1,1,1) to (1.5,1.5,1.5) and (B) from (1.5,1.5,1.5) to (2,2,2), and at different energies and modes of operation, as indicated. In every case an anomaly is visible at $aq/2\pi\approx 0.75$. The measurements in each series, indicated by a symbol, were made successively using the constant $\mathbf{Q}$ method. One set of results are shown in Fig. 4.

The Fermi surface of lead contains four electrons, and, therefore, on the free electron model, has a radius

[21] See J. M. Ziman, *Electrons and Phonons* (Oxford University Press, New York, 1960).

[22] A. V. Gold, Phil. Trans. Roy. Soc. London **A251**, 85 (1958).

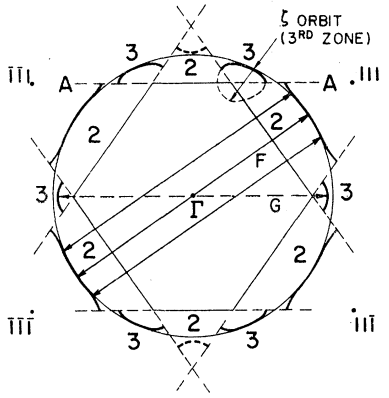

FIG. 10. Possible section through the Fermi surface of lead in a $(1\bar{1}0)$ plane through the origin. The section of the free electron sphere containing four electrons is shown as a light circular line. Bragg reflection occurs where this circle intersects the reflecting planes shown, and the Fermi surface is distorted somewhat as shown. Electron scattering vectors which produce a Kohn anomaly in the $[\zeta\zeta\zeta]$ L branch are indicated by the bold double headed arrows, F, and in the $[\zeta\zeta 0]$ L branch by the dashed double headed arrow, G.

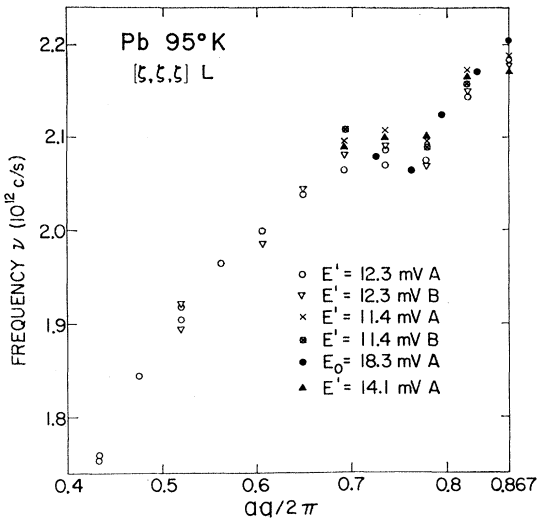

FIG. 11. Collected results for the $[\zeta\zeta\zeta]$ L branch. The letters A and B refer to zones about the (1,1,1) and (2,2,2) reciprocal lattice points.

$K_F = 1.2407(2\pi/a)$. From Eq. (9), an anomaly due to transition F would occur in the $[\zeta\zeta\zeta]$ L branch at

$$|\mathbf{q}| = 2K_F - 2\pi|\tau| = (2.4814-1.732)(2\pi/a) = 0.75(2\pi/a).$$

Thus, if we identify the observed anomaly as this Kohn anomaly F, the Fermi radius along the body diagonal [111] differs from the free electron Fermi radius by at most 1%, and is probably slightly larger.

Figure 12 shows the $[\zeta\zeta 0]$ L branch, also measured at several regions in reciprocal space. For free electrons an anomaly due to transition G is expected at $|\mathbf{q}| = (2.8283-2.4814)(2\pi/a) = 0.347(2\pi/a)$. If we identify this Kohn anomaly with the observed[23] anomaly at $0.45(2\pi/a)$, then the Fermi diameter along the face diagonal [110] is found to be $2.38(2\pi/a)$, 4% smaller than for free electrons. The difference is in the expected direction since this part of the Fermi surface is beyond, but close to, Bragg reflecting planes [see Fig. 10]. It is in qualitative agreement with the de Haas-van Alphen measurements of Gold,[22] which show a closely related orbit (the ζ orbit in the third zone—see Fig. 10) to be 30% smaller than for free electrons; this corresponds to a 4 or 5% decrease in the Fermi diameter in the extended zone scheme.

The signs of the anomalies F and G of Figs. 11 and 12 are compatible with the rule[3,20]: "As the phonon wave vector in the extended zone scheme exceeds the Fermi diameter, the abrupt decreased shielding of the ions by the electrons causes the frequency to increase anomalously."

The assignment of the anomaly of Fig. 11 was checked once by making measurements along a line parallel to the $[\zeta\zeta\zeta]$ direction from $\mathbf{Q}(a/2\pi) = (1.4,1.4,1.15)$ to (1.85,1.85,1.6) at intervals in ζ of 0.025. Similar small anomalies were seen on opposite sides of the zone boundary [(1.583,1.583,1.333)] at approximately (1.525,1.525,1.275) and (1.64,1.64,1.39), as expected for a "longitudinal" anomaly such as F. [If the anomaly were "transverse," involving electron momentum transfers not parallel to $\mathbf{q}$, then in off-symmetry directions it would not appear symmetrically about the zone boundary.]

The magnitudes of the anomalies are of the same size as the absolute errors expected in the experiments. However, the experiments were carried out in consistent ways such that many of the errors (e.g., of calibration and of specimen alignment) entered in the same way

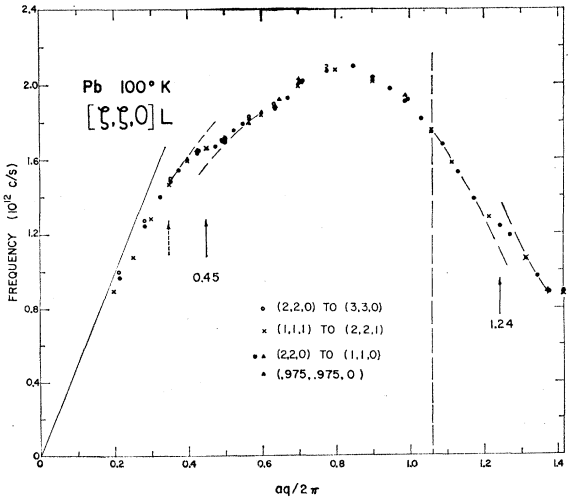

FIG. 12. Collected results for the $[\zeta\zeta 0]$ L branch, showing an anomaly at $aq/2\pi = 0.45$, and a probable one at 1.24.

[23] The construction used to locate the position was suggested by S. H. Vosko (private communication).

for all the points in a given series. The random errors expected from statistics are much smaller than the expected absolute errors or than the magnitudes of the anomalies. We can estimate the statistical errors in locating the center of a neutron group by the expression.

$$\Delta\nu \approx N^{1/2}n^{-1/2}d\nu/dN.$$

N (the number of counts per point) has typical values of 100 or so, n (the number of points in a peak) is usually about 10, and $d\nu/dN$ is typically 2×10^9. Thus, the statistical uncertainty in a frequency is ordinarily less than 10^{10} cps, several times smaller than the anomalies. The anomalies could possibly be spurious if there existed unrecognized contaminant structure in the energy distributions. To eliminate this hazard as far as possible the measurements were repeated at several different energies (Fig. 11) and at different positions in reciprocal space (Figs. 11 and 12). In every case an anomaly was observed at about the same position.

From another point of view the Kohn anomalies result from interatomic forces of very long range and of varying sign (cf. the work of Langer and Vosko[24] on the screening in metallic alloys). This is just the behavior already discussed in Sec. III. The Fourier components needed to reproduce the anomalies of Figs. 11 and 12 are of considerably shorter wavelength (and therefore represent forces of longer range) than those obtained in the fits of Table IV which reproduce the over-all shape of the dispersion curves. Thus, the Kohn anomalies require only an extension to greater distances of the already long-range forces certainly needed to explain the over-all behavior of the dispersion curves.

Note added in proof. The anomalies discussed above have now been observed in x-ray scattering by A. Paskin and R. J. Weiss [Phys. Rev. Letters **9**, 199 (1962)].

2. Theory

We will discuss the Kohn effect in terms of calculations made by Toya[19] for the case of nearly free electrons, using the Hartree-Fock method. Toya solved the Hartree-Fock equation for the metal in the presence of the lattice vibrations to obtain the electronic energies. These energies then were used (the adiabatic approximation) in the potentials for the ions, and the lattice vibrations calculated. In Toya's work (which actually preceded Kohn's) the Kohn effect is explicitly displayed, although Toya did not comment on its existence and indeed the effect turns out to be very small for nearly free electrons.

The Kohn effect enters via the electron-phonon interaction, in the theory through the matrix element given by Bardeen.[25] The matrix element involves energy denominators in the form of a sum,

$$W^{-1}=\sum_{\mathbf{k}_e}[E_e(\mathbf{k}_e)-E_e(\mathbf{k}_e+\mathbf{K})]^{-1}, \tag{10}$$

where $\mathbf{K}=2\pi\boldsymbol{\tau}+\mathbf{q}$, $\mathbf{k}_e$ is the wave vector of an electron and E_e is the corresponding energy. For free electrons, the summation yields[25]

$$W^{-1}=-(3N/4E_F)f(t), \tag{11}$$

where the reduced wave vector transfer $t=K/2K_F$, E_F is the Fermi energy, N is the number of electrons per unit volume, and the function

$$f(t)=\tfrac{1}{2}+\frac{1-t^2}{4t}\ln\left|\frac{1+t}{1-t}\right| \tag{11a}$$

is shown in Fig. 13(b).

The frequency eigenvalues $M\omega^2$ are given by the algebraic sum of several terms, one of which takes account of the shielding of the motions of the ions by the electrons. Neglecting exchange and correlation (taken into account in an approximate way by Toya), this term is proportional to a factor

$$f(t)[2\pi e^{-2}K_F^{-1}E_Ft^2+f(t)]^{-1}. \tag{12}$$

The Kohn anomalies occur[7] at $t=1$, at which point the slope of $f(t)$ is logarithmically infinite. The infinity in the slope strictly occurs only over an infinitesimal range in f (and therefore in the frequency), and is thus unobservable. The anomaly appears in practice in the form of high (but not infinitely high) Fourier components.

The anomalies are reduced by another factor in the matrix element—the overlap integral coming from the perturbation. Physically, this factor—a kind of form factor—arises because the electrons are spread out in space: correspondingly the electrons cannot experience large momentum transfers, and thus cannot interact with lattice waves of large wave vector (in the extended zone scheme).

If the Bloch wave functions of the electrons are approximated as $U_0(\mathbf{r})\exp(i\mathbf{k}_e\cdot\mathbf{r})$, with U_0 independent of $\mathbf{k}_e$, the matrix element is proportional to the square of a factor

$$g(KR_s)=\int U_0^*\exp(i\mathbf{K}\cdot\mathbf{r})U_0d\mathbf{r}, \tag{13}$$

where the integral is taken over the Wigner-Seitz cell of equivalent radius R_s. For nearly free electrons ($U_0\sim1$)

$$g(x)=3x^{-3}(\sin x-x\cos x). \tag{14}$$

The factor g^2 for free electrons is shown in Fig. 13(a). For Na, the Kohn anomalies ($K=2K_F$) occur at the position of the arrow; the amplitude of the anomaly is thus markedly decreased[20] by this factor. For Pb, on the free electron model, the anomalies would occur at

[24] J. S. Langer and S. H. Vosko, J. Phys. Chem. Solids **12**, 196 (1959).
[25] J. Bardeen, Phys. Rev. **52**, 689 (1937).

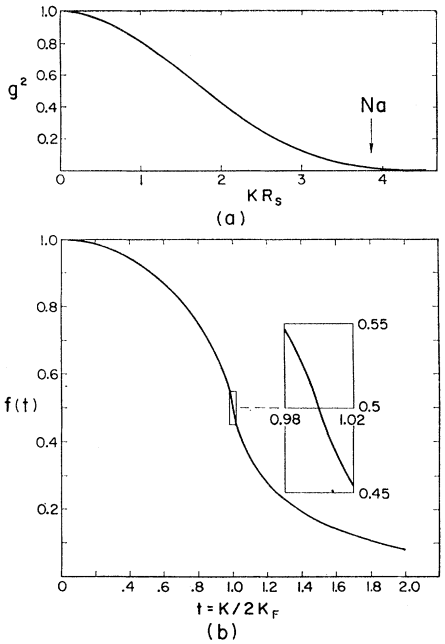

FIG. 13. (a) The "form factor" for free electrons; (b) the "energy denominator" for free electrons.

$KR_s = 6.07$ for which $g^2 \approx 6 \times 10^{-3}$, and thus would be probably unobservable.

The free electron model is not adequate for Pb, however. Specific-heat measurements[26] show that the mean density of states at the Fermi surface is about twice that for a metal with four free electrons if the area of the Fermi surface is taken equal to that for free electrons. Rf conductivity measurements[27] show that the Fermi surface has an area only 55% of the area of the Fermi surface for free electrons. Thus the density of states at the actual Fermi surface is larger than that for free electrons by about 2/0.55, a factor of more than 3. The amplitudes of the Kohn anomalies are proportional to the products of two densities of states (at the initial and final states), as can be seen from Eq. (10). Thus, *on the average* the Kohn anomalies in Pb will be enhanced by over an order of magnitude, and the enhancement could be greater still, since the density of states will be far from uniform over the Fermi surface.

In Pb also the wave functions of the electrons must be considerably different from uniformly spread-out free electrons, and should be expected to be rather concentrated about the nucleus. Then, by Eq. (13), the factor g^2 would be correspondingly enhanced at large momentum transfers. On crude computations it does not seem difficult to obtain an enhancement of over an order of magnitude.

Thus it seems possible to account qualitatively for the observation of the Kohn effect in Pb, despite the expected weakness of the effect for free electrons.

It is attractive to try to explain the drop in frequency of the $[\zeta 00]$ L branch at the zone boundary, as arising from an enormous Kohn anomaly. We would then look for electron transitions between regions of high density of states with small momentum transfer. The strong anomaly in the $[\zeta\zeta 0]$ L branch at $aq/2\pi \simeq 1.24$ [Fig. (12)] is tentatively ascribed to transitions along the line $A-A$ in Fig. (10). (These anomalies would not occur for free electrons). The $[\zeta 00]$ L anomaly might then arise from similar transitions in the [100] directions of the plane normal to the plane of Fig. (10), and intersecting it in line $A-A$. This would require a large distortion of the free electron Fermi surface in the third zone.

V. CONCLUSIONS

The results of this paper have demonstrated that the dispersion curves of metals contain a great deal of detailed information about the electronic structure of the metal, including details of the Fermi surface. By use of the Kohn construction, it is possible to study the Fermi surface. (It should be noted that this method of studying Fermi surfaces is one of the few useable at elevated temperatures.) There is, however, much information about other aspects of the electronic structure available if ways can be found to extract it.

ACKNOWLEDGMENTS

We wish to thank Dr. J. M. Kennedy for help in computing problems, M. Sakamoto and Dr. R. N. Sinclair for assistance in taking some of the data, A. Bell and E. A. Glaser for technical assistance, and Dr. S. H. Vosko for helpful discussions.

[26] See J. G. Daunt, in *Progress in Low-Temperature Physics*, edited by C. J. Gorter (North-Holland Publishing Company, Amsterdam, 1955), Vol. I, Chap. XI.

[27] J. E. Aubrey, Phil. Mag. 5, 1001 (1960).